RSC Advances

ROYAL SOCIETY OF CHEMISTRY

www.rsc.org/advances

A comparative study on the morphological features of highly ordered MgO:AgO nanocube arrays prepared via hydrothermal method

K. Kaviyarasu[1,2*], E. Manikandan[1,2,3], J. Kennedy [1,2,4], M. Maaza[1,2]

[1]UNESCO-UNISA Africa Chair in Nanosciences/Nanotechnology Laboratories, College of Graduate Studies, University of South Africa (*UNISA*), Muckleneuk Ridge, P O Box 392, Pretoria, South Africa.

[2] Nanosciences African network (*NANOAFNET*), Materials Research Department (MSD), *i*Themba LABS-National Research Foundation (*NRF*), 1 Old Faure Road, 7129, P O Box 722, Somerset West, Western Cape Province, South Africa.

[3]Central Research Laboratory, Sree Balaji Medical College & Hospital (SBMCH), Bharath University, Chrompet, Chennai-600044, Tamil Nadu, India.

[4]National Isotope Centre, GNS Science, PO Box 31312, Lower Hutt 5010, New Zealand.

ABSTRACT

II–VI semiconductor nanotubes are recently developed class of nanomaterials whose unique photo-physical properties are helping to create a new generation of nanomaterials in the field of photonics and microelectronics. In this report, we examine the progress in adapting these nanomaterials for several optoelectronics application followed by characterization studies. Magnesium oxide and silver oxide (MgO:AgO) nanoparticles were synthesized using hydrothermal method by taking magnesium nitrate, silver oxide and glycine. X-ray diffraction (XRD) results showed that the peaks are consistent with pure phase cubic structure of MgO. The XRD pattern also confirmed crystallinity and phase purity of the sample. Nanocrystals sizes were

[1] Corresponding authors: kaviyarasuloyolacollege@gmail.com (K. Kaviyarasu); likmaaza@gmail.com (M. Maaza), Tel:- +27630441709.

found to be up to 25 nm as revealed by XRD and HRTEM. Photoluminescence measurement (PL) reveals the systematic shift of the emission band towards lower wavelength thereby ascertaining the quantum confinement effect.

Keywords: Nanoparticles; Composite materials; Semiconductor; PL; μ-Raman.

1. Introduction

Nanoparticle systems in recent time have attracted considerable interest from both academia and industry because of their interesting and diverse properties, which deviate from those of the bulk. Owing to the change of properties, the fabrication of nanostructural materials and devices with unique properties in atomic scale has become an emerging interdisciplinary field involving materials science, solid-state physics, chemistry and biology [1]. The synthesis of silver oxide (AgO) nanoparticles with well-defined size, size distribution, morphology, and crystallinity becomes increasingly important for advances in the field of nanotechnology, in particular for selective catalysts or self-assembled patterns [2]. Magnesium oxide (MgO) is a typical wide band gap (7.2 eV) semiconductor, which represents an important class of functional metal oxides with a broad range of properties. It also finds tremendous application in catalysis, refractory industries, electronics, cosmetics and waste water remediation. MgO exhibits excellent performances in high temperature, particularly in the creation of electrical insulation [3]. Other properties of MgO include effective corrosion resistance and transparency to IR light. It has a high thermal and low electrical conductivity. MgO is thermodynamically stable and is often used as a buffer layer in superconductor and ferroelectric materials. The vast applications of MgO

nanomaterial has led to study of MgO in various morphologies such as nanorods, nanobelts, nanowires, nanosheets, and nanoplates which have been synthesized via a variety of different chemical routes [4-9]. By combining these metals into a single entity, catalytic properties can be further enhanced and localized surface plasmon absorption can be varied continuously between the limits of monometallic MgO and AgO nanoparticles [10]. AgO nanocube has the highest electrical conductivity among all the metals, by virtue of which AgO nanocubes are considered as very promising candidates in flexible electronics. Several methods have been used to produce AgO nanoparticles. The most common one is the co-reduction of the metal precursors in the presence of a stabilizing agent or in water-in-oil micro-emulsions [11]. A number of studies were performed by researchers around the world. The results reveal that isolated nanoparticles and substrate-supported nanoparticles with relatively free surfaces usually exhibit a significant decrease in melting temperatures as compared to conventional bulk materials. The physical origin for this phenomenon is that the ratio of the number of surface-to-volume atoms is enormous, and the liquid/vapor interface energy is generally lower than the average solid/vapor interface energy. Therefore, as the particle size decreases, its surface-to-volume atoms ratio increases and the melting temperature decrease as a consequence of the improved free energy at the particle surface.

2. Experimental Procedures

2.1 Chemicals & Sample characterization techniques

All chemical reagents used in this experiment were of analytical grade (E-Merck, 99.99%), were procured commercially and used without further purification. The starting materials for the

preparation of MgO doped AgO nanomaterials were synthesized by taking magnesium nitrate [$Mg(NO_3)_2$], silver oxide, (AgO) and glycine [NH_2CH_2COOH] in the appropriate stoichiometric ratio. The calculated amount of glycine was first dissolved in deionized water. $Mg(NO_3)_2$ was then added to the solution slowly by stirring, maintained at 185 °C. The homogeneous mixture obtained was filtered out using ultra-fine filter paper and heated with an electrical heating mantle for five hours. N_2 and CO_2 evolved as bright dark yellow gas mixture and MgO was left behind as the end residue. The synthesized nanopowder was annealed at 900 °C in a microprocessor controlled single zone furnace for 15 hours, thereby resulting in good quality MgO nanocube. The final products were characterized by X-ray diffraction (XRD) and data were recorded employing Rich Seifert diffractometer using Cu K_α (λ=1.5418 Å) with diffraction angle 2θ values ranging from 20° to 80°. A UV-vis-NIR spectrum was recorded in the region 200 - 1200 nm using VARIAN CARRY 5E model UV-Vis-NIR spectrometer. The photoluminescence measurements were performed on a Jobin Yvon Flurolog-3-1 Spectroflurometer using 3 nm slit width. The emission was collected and sent to a Jobin-yuon Triax monochromator and detected by a Hamamastsu Ra28 photomultiplier tube. The thermo gravimetric analysis (TGA) and differential thermal analysis (DTA) were carried out using NETZSCH STA 409C thermal analyzer at a heating rate of 20 °C/min in the nitrogen atmosphere to determine the thermal stability of the compound between room temperature and 375 °C. The XPS spectrum was recorded on a ESCALAB 250 photoelectron spectrometer (Thermo-VG Scientific, USA) with Al K_α (1486.6 eV) as the X-ray source. A Renishaw micro-Raman spectrometer RM 2000 with IR (632.8 nm) and UV (325 nm) excitation lasers was employed to measure the non-resonant and resonant Raman spectra of MgO:AgO samples.

3. Results and discussion

3.1 X-ray Powder Diffraction

X-ray diffraction (XRD) studies were carried out to confirm the crystallinity phase and the spectrum is shown in Figure 1. The spectrum reflects the good crystallinity for both pure MgO and doped MgO:AgO samples. The broadness of the XRD peaks indicates the nanocube nature of pure and doped MgO:AgO nanoparticles. The Bragg's reflections are indexed in MgO like cubic structure and the estimated cell constant is (a = 4.21 Å) of MgO particles confirming that the sample is formed in a single phase. The cell constant is slightly less than that of MgO nanosamples which may be due to the introduction of silver in MgO (a = 4.38 Å). Considerably broadened lines in the XRD patterns are indicative of the presence of nano-size particles. We have used the (111) reflection, like in the XRD patterns, to estimate the average particle size with help of Debye–Scherrer's equation, $D = 0.9\ \lambda/\beta \cos\theta$, $B = (B^2_M - B^2_S)^{1/2}$ where 'D' is the size of the particle, λ is the X-ray wavelength (1.5418 Å), B_M and B_S are respectively the measured peak broadening and the instrumental broadening in radian and 'θ' is the Bragg angle of the reflection. The calculated average particle size MgO:AgO nanosamples was 25 nm. The XRD pattern of regenerated MgO powder ascertains MgO and the Ag doped MgO samples.

3.2 Optical absorption spectral analysis

The optical absorption spectral studies are carried out to detect the lower concentration of defects rather than the optical absorption. This is a mechanism where the impurity on absorption of light, gives rise to the bound excited state from which it returns to its ground state abiding in

accordance with the color center creation mechanism. The room temperature photoluminescence spectrum of MgO:AgO nanocubes is shown in Figure 2. When the excitation wavelength is 190 nm, the peaks are observed at 235 nm and 438 nm, respectively. The absorption spectrum of MgO:AgO nanocube shows two distinct absorption peaks. The appearance of minor peak at 235 nm corresponds to n-π* transition and the major peak with maximum absorption at around 438 nm represents the π-π* transition. The absorption peak λ max value is in agreement with the λ max of 438 nm, whereas the addition of silver nanoparticles resulted in the formation of a peak centered at 438 nm. It is well known that it exhibits a surface plasmon resonance band between 350 nm and 450 nm, and presence of band confirms the formation of silver nanoparticles within the matrix. The peak at 235 nm can be attributed to the relaxation of polarization defects formed by the strained sites attached to oxygen vacancies. Oxygen vacancy might be the common defect in the nanosamples which induces distortion of the lattice in its direct surrounding. In case of current samples, the red shift in the MgO is slightly enhanced. Therefore, red shift of the photoluminescence peaks is likely to be a result of band gap reduction. Such characteristic is vital for enhancement of secondary electron emission efficiency, reduction of flickening etc. Therefore the optical property is promising for its application in plasma display panels (PDP) or other optoelectronic devices.

3.3 Photoluminescence Spectra

Figure 3 shows the PL spectrum of MgO:AgO nanocube which has PL peak at about 532 nm. The luminescence curve from the surface states around 480-550 nm has also been observed. The peak of eigen-transistion is strong and narrow and the emission of surface is seen with minor

humps indicating the quantum confinement effect. Thus the PL spectrum is dominated by a strong and narrow band edge emission tunable in the blue region of the visible spectrum, indicating a narrow size distribution of MgO nanocube. This band edge is possibly comprised of recombination of luminescence of shallow traps or surface defects localized excitions and intrinsic excition. The large band at about 352 nm can be attributed to radiative recombination from deep defect and impurity levels. Takahashi et al. [12] reported that the deep level defects in MgO are usually created by impurities and vacancy complexes lie in 1.4 - 4.6 eV. Perera et al. [13] found that this band can be present in MgO microcrystals and centered at 2.8 eV. These authors have associated the above bands to Mg interstates.

3.4 Thermal Analysis Test

The thermo gravimetric analysis (TGA) and differential thermal analysis (DTA) were carried out using NETZSCH STA 409C thermal analyzer at a heating rate of 20 °C/min in the nitrogen atmosphere to determine the thermal stability of the compound between room temperature and 375 °C. The resulting TGA/DTA trace is shown in Figure 4. A careful examination reveals that the major exothermic peak around 80.90 °C could be due to absorption of water molecules. A steady decrease in the weight observed up to 375 °C (53.37%) may be due to the decomposition of the sample. The DTA curve shows a sharp endothermic peak at 101.62 °C which corresponds to the melting point of the compound. A very broad and sharp exothermic peak observed at 229.49 °C and 308.31 °C indicate a change in the physical state of the crystallite size and luminescence property.

3.5 μ-Raman studies

The Raman spectrum of the pure MgO:AgO nanocubes in the 250-1750 cm^{-1} region was recorded by RENISHAW which is a high performance Raman microscope spectrometer using a 632.8 nm diode lasers. Figure 5 shows the Raman spectra of MgO:AgO nanocubes which revealed distinct peaks at room temperature (RT). First sharp peak appears at 375 cm^{-1} which is not existent in pure MgO nanocube. But when silver is added, D band (*785 cm^{-1}*), G band (*815 cm^{-1}*) and 2D band (*1456 cm^{-1})* appeared in the Raman spectra. The area under the Raman peak changed with the silver percentage and increased with higher concentration, probably due to silver in induced surface roughness to identify the UV and PL images.

3.6 HRTEM and SAED analysis

The HRTEM images for the pure MgO:AgO samples are shown in Figure 6 (a–f). MgO:AgO aggregates consist of very tiny three dimensional (3D) disordered primary nanoparticles with interplanar connections well arranged in the series of chains due to the attractive forces between nanoparticles as shown in Figure 6 (a, b). At the same time the particles of the magnesium–silver nanocomposites looked less aggregated than that one's of the initial nanosilver powder Figure 6 (c, d). The HRTEM studies of the MgO:AgO nanocomposites morphology revealed the that the silver nanocube with average diameter of 20 nm are surrounded with magnesium nanoparticles of 5 nm that kept the nanosilver together like connected in the chains Figure 6 (e). The particles size measured by HRTEM is in a good agreement with the calculation made according the XRD data. The SAED patterns to analysis of the crystalline phases obtained after calcinations at room temperature (RT) are shown in Figure 6 (f). The diffraction peaks were very diffused suggesting that the texture is quite polycrystalline with small grain size [14]. Therefore the distributed pore sizes and the mean pore diameter obtained

from the N_2 adsorption–desorption analysis would represent the exact values of the whole samples. It should be mentioned that particles size of magnesium obtained in presence of nanosilver are rather small even in absence of any additional stabilizing agents. Even for the most important part of the magnesium nanoparticles deposited on the silver. Since the Ag is a known catalyst for redox reactions, it can indicate that silver catalyses the reaction of magnesium formation [15]. Based on the fact that surface of silver nanoparticles is not completely covered with magnesium, one can assume the possibility of coordinating silver and magnesium sites with different type of ligands like (–Mg) or (–COOH) that can be used in optoelectronic devices The total content of Ag in the sample is 4.1 wt% that corresponds to 5.3 wt% of magnesium.

3.7 XPS analysis

Figure 7 shows the XPS wide scan spectra of MgO:AgO nanocube in the binding energy ranging up to 250 to 1300 eV. It can be seen that the nanocube contains Mg and O elements along with a peak associated with carbon. Two peaks at 532 eV and 1253 eV for O 1s and Auger peaks, respectively, were identified and each component peak in the spectrum was fitted with Lorentzian function. The major peak of lower binding energy was assigned to lattice oxygen (Mg-O-) in the MgO:AgO nanocube , while the smaller peak of higher binding energy was assigned to the hydroxyl group of oxygen, which is very common in samples with high surface energy. This may be due to the variation of the lattice constants a & c (a = 0.387 nm; c = 0.485 nm, which are calculated from XRD pattern). Together with the shrinking of lattice for MgO:AgO nanocube, suggests that the oxide anions form octahedral of magnesium enclosing the

silver ions and the Mg-O bonds in lattice become much more stronger. This result reveals that the lattice shrinkage plays a significant role in the spin-orbit splitting of Mg 2*p* state.

3.8 Confocal laser scanning microscopic studies

The polarization dependence and the effect of fluorescence of pure and magnesium doped silver oxide nanoparticles were visualized by confocal laser scanning microscopic studies. This is a mechanism where the impurity on absorption of light, gives rise to the bound excited state from which it returns to the ground state abiding in accordance with the color center creation mechanism. The room temperature optical spectra of pure MgO:AgO nanosamples are shown in Figure 8. Optical images in reflectance mode images were yellowish-orange bright spots with sizes up to 50 μm, with a higher density in Figure 8 (a) show a fully developed luster with a nice gold metallic shine. Figure 8 (b) shows a higher reflectance at the edges than at the center of the luster decorations. The edges appear bright orange and contain some highly reflecting yellowish-orange spots whereas the center shows a lower reflectance and orange-yellow color. Figure 8(c) exhibits a highly reflecting gold-like edge and an orange-yellow color. It is interesting to notice the presence of scattered blue spots on samples (figure 8 (b&c)) which correspond to accumulations of metallic silver particles. Optical images cross section micrograph obtained in transmission mode in bright field from the ion-thinned glaze during TEM sample preparation showing a red line at the glaze surface corresponding to the lustre decoration layer. The studies indicate that the fluorescence generated by MgO doped AgO nanoparticles shows a change in fluorescence in the solid state along the vortex region. The pattern generated by the fluorescent light could be useful in the applications such as biological marking. Moreover, the spectrum of our MgO:AgO nanocube is different from that of the nanoparticles synthesized by wet-chemical

method which shows the band broadening with decrease in intensity. This difference can be attributed to the effect of smaller particle size, which affects the force constant and vibrational amplitudes of the nearest neighboring bond.

3.9 Electrochemical behavior of MgO:AgO

The first scan shows a reduction wave at the potential of 0.15 V, which can be attributed to the Ag+ ions deposition onto the surface of NaOH electrode. A large irreversible cathodic peak was observed at −1.05 V in the potential range from +1.5 V to −1.5 V. This current wave can be ascribed to the reduction of surface bounded oxygenated functional groups on the AgO nanocube, such as OH, Mg-O-Ag on the plane and COOH on the edges. It is also noticeable that the reduction peak current decreased dramatically in the second cycle and disappeared after several potential scans, indicating that most of the available oxygenated groups were electrochemically reduced during the first scan. According to the Faraday's law of electrolysis and the reduced peak area in the first cycle, we can estimate that there were 8799 of oxygenated group's subsequent scans at peak potential at 0.2 V. This phenomenon could be explained by the deposition of silver on the existing silver nuclei formed during the first cycle. To ensure an efficient reduction for producing silver seeds, the nucleation potential was chosen at 0.13 V smaller than the reduction peak potential (0.15 V). And meanwhile, because of the kinetic priority of progressive nucleation, the pulse length of nucleation process was set to an extremely short time (5 ms) to make an instantaneous nucleation. Growth potential was carefully chosen at the foot of the silver plating wave (0.25 V) to avoid the stripping of Ag NCs and to suppress the second nucleation usually resulting in polydisperse nanomaterials. Figure 9 shows a current-time

transient curve of Ag+ ions electrodeposition following the above optimized conditions. After an initial decaying charging current, an increasing cathodic current was followed and reached to a maximum value. A decaying current was finally recorded due to individual spherical diffusion zones around the silver nuclei.

3.10 Dielectric Studies

Dielectric measurements on carefully cut and polished MgO:AgO nanosamples of synthesized nanocube were carried out using HIOKI 3532-50 LCR Hi TESTER in the frequency range of 100 Hz to 10 MHz. A sample of nanocube with dimension a=0.387 nm, c = 0.485 nm, having silver coating on the opposite faces was placed between the two copper electrodes to form a parallel plate capacitor [16-19]. Figure 10 shows the plot of dielectric constant (ε') versus applied frequency. From the graph it can be seen that the dielectric constant decreases, indicating that the MgO:AgO nanocube possess improved electrochemical properties. The dielectric loss is studied as a function of frequency for various temperatures and is shown in Figure 10. These curves suggest that the dielectric loss is strongly dependent on the frequency of the applied field similar to that of the dielectric constant [20]. The V-I characteristics of the MgO:AgO nanocube at room temperature using four probe method is shown in Figure 10 (c). From the graph, the resistivity and the conductivity of the MgO:AgO nanocube is found to be 6800 Ωm and 1.47×10^{-4} Sm^{-1}, respectively.

3.11 Atomic force microscopic studies

Height calibrations were performed using the step heights of freshly cleaved MgO:AgO nanosamples. Due to the super-roughness of the samples, sometimes the laser interference pattern along the slow-scan axis was hard to avoid, which is more noticeable in large-area scanning and has a period of twice the wavelength of the laser. This is caused by the constructive interference of laser reflected from the sample surface and that reflected from the cantilever. The nanosamples investigated in this work have been obtained by the micromechanical behavior of MgO:AgO nanocube which were mechanically exfoliated and transferred of this silicon wafer and covered with 5.04 μm of thermal oxide. We identified the single and spherical shapes by the color influence in the optical microscope. The MgO:AgO nanocube were imaged by the atomic force microscopy (AFM) to ensure the uniformity of the surface layer. Figure 11 (a-c) shows a typical AFM image of the MgO:AgO nanolayers on a silicon substrate, which were used for this study. After AFM quality control, the MgO:AgO nanocube on silicon substrates were transferred under the optical microscope connected to the area profile curve (shows the actual spots from which the 1 μm × 1 μm data were collected). To confirm this mapping was performed on large surface nanocube before and after at RT. AFM surface analysis requires close attention since many factors can lead to erroneous results such as the presence of deformation or even the presence of artifacts in the image due to the tip and/or contamination. In contact mode, the probe is placed in contact with the surface. In this case, the force between the tip and the sample can cause irreversible damage to the magnesium and the silver oxide nanocube. Thus, it is appropriate to use only the non-contact mode in this work, since in the non-contact mode the tip is placed very close to, but not in contact with, the sample. The area analyzed was 1 μm × 1 μm. It can be seen in the surface images that the topography of the silver is fairly regular in figure 11 (a). The image of a profile in figure 11 (b) was traced in the topography, which shows a small

variation (of the order of 10.5 μm) in the surface topography of the MgO:AgO nanocube . The formation of layers of three-dimensional spherical clusters, after metallization, corresponds to silver nanoparticles in the sense of their plasmonic behavior. This result is consistent with the little definition of cluster size for layers less than 10.5 μm, possibly due to the mobility of silver atoms on the surface of the magnesium. In fact, in some experiments it was not possible to distinguish the silver from the magnesium, but the surface morphology is quite distinct from the sample without the magnesium on silver as shown in figure 11 (a). For nanocube of 10.5 μm (figure 11 (c)), the presence of larger clusters is shown and better defined due to the large amount of silver deposited. Even though the images presented in Figure 11 (a&b) display a clear variation on the grain size, a grain by grain measurement was performed in order to obtain a more reliable average grain size for each silver oxide nanocube width.

4. Conclusions

In summary, we successfully synthesized of MgO:AgO nanocube using hydrothermal method. The XRD pattern shows the MgO:AgO nanosamples were pure cubic phase crystallinity structure. XRD and HRTEM revealed the nanocrystals were formed with sizes up to 25 nm. XPS results showed presence of Mg and O in the sample. The phenemenonal increase in the absorption spectrum due to doping the broad band in MgO doped nanopowders has slightly increased gradually. Thus this method can be potentially extended to the future preparation of other metal oxides including CdO, PbO and TiO_2 nanostructures for optoelectronic applications.

Acknowledgements

The authors gratefully acknowledge research funding from UNESCO-UNISA Africa Chair in Nanosciences/Nanotechnology Laboratories, College of Graduate Studies, University of South Africa (UNISA), Muckleneuk Ridge, Pretoria, South Africa, (Research Grant Fellowship of framework Post-Doctoral Fellowship program under contract number Research Fund: 139000). One of the authors (***Dr. K. Kaviyarasu***) is grateful to **Prof. M. Maaza**, Nanosciences African network (NANOAFNET), Materials Research Department (MSD), *iThemba* LABS-National Research Foundation (NRF), Somerset West, South Africa through Support Program and the Basic Science Research Program through the National Research Foundation of South Africa for his constant support, help and encouragement generously.

Reference

[1] A. Cho, K.Y. Cheng, Growth of extremely uniform layers by rotating substrate holder with molecular beam epitaxy for applications to electro-optic and microwave devices, Appl. Phys. Lett. 38 (1981) 360-362.

[2] S.H.C. Liang, I.D. Gay, A ^{13}C solid-state NMR study of the chemisorption and decomposition of ethanol on MgO, J. Catal. 101 (1986) 293-300.

[3] P. Yang, C.M. Lieber, Nanorod-Superconductor Composites: A Pathway to Materials with High Critical Current Densities, Science 273 (1996) 1836-1839.

[4] Y. He, Preparation of polyaniline/nano-ZnO composites via a novel Pickering emulsion route, Powder Technol. 147 (2004) 59-63.

[5] K. Kaviyarasu, C. Maria Magdalane, K. Anand, E. Manikandan, M. Maaza, Synthesis and characterization studies of MgO:CuO nanocrystals by wet-chemical method, Spectrochimica Acta Part A: Mol. & Biomol. Spect. 142 (2015) 405-409.

[6] K. Kaviyarasu, E. Manikandan, P. Paulraj, J. Kennedy, One dimensional well-aligned CdO nanocrystals by solvothermal method, J. Alloys & Comp. 593 (2014) 67-70.

[7] K. Kaviyarasu, J. Kennedy, E. Manikandan, Synthesis of Mg doped TiO_2 nanocube prepared by wet-chemical method: Optical and microscopic studies, Int. J. Nanosci. 12 (2013) 1350033.

[8] K. Kaviyarasu, D. Sajan, M.S. Selvakumar, S. Augustine Thomas, D. Prem Anand, A facile hydrothermal route to synthesize novel PbI_2 nanorods, J. Phys. & Chem. Sol. 73 (2012) 1396.

[9] K. Kaviyarasu, E. Manikandan, J. Kennedy, M. Jayachandran, Quantum confinement and photoluminescence of well-aligned CdO nanofibers by a solvothermal route, Mater. Lett. 120 (2014) 243-245.

[10] J.A. Farmer, C.T. Campbell, L. Xu, G. Henkelman, Defect Sites and Their Distributions on MgO (100) by Li and Ca Adsorption Calorimetry, J. Am. Chem. Soc. 131 (2009) 3098-3103.

[11] M.S. Melgunov, V.B. Fenelonov, A partial surface area measurement method for multicomponent catalysts and adsorbents, React. Kin. Cat. Lett. 64 (1998) 153-160.

[12] S. Takahashi, Y. Imai, A. Kan, Y. Hotta, H. Ogawa, Improvements in the temperature-dependent properties of dielectric composites by utilizing MgO whiskers as the dielectric filler in an iPP matrix, J. Alloys & Comp. 640 (2015) 428–432.

[13] D.C. Perera, W.J. Hewage, N.D. Silva, Theoretical study of catalytic decomposition of acetic acid on MgO nanosurface, Comp. Theoretical Chem. 1064 (2015) 1–6.

[14] H.X. Mai, L.D. Sun, Y.W. Zhang, R. Si, W. Feng, H.P. Zhang, H.C. Liu, C.H. Yan, Shape-selective synthesis and oxygen storage behavior of ceria nanopolyhedra, nanorods, and nanocubes, J. Phys. Chem. B 109 (2005) 24380–24385.

[15] R. Inguanta, S. Piazza, C. Sunseri, Template electrosynthesis of CeO_2 nanotubes, Nanotechnology 18 (2007) 1–6.

[16] M. Veerapandian, S.K. Lim, HM. Nam, G. KuppannanK. S. Yun. Glucosamine Functionalized Silver Glyconanoparticles: Characterization and Antibacterial Activity, Anal. & Bioanalyt. Chem. 398 (2010) 867–876.

[17] K. Kaviyarasu, Prem Anand Devarajan, Synthesis and characterization studies of cadmium doped MgO nanocrystals for optoelectronics application, Adv. App. Sci. Res. 2 (2011) 131-138.

[18] K. Kaviyarasu, Prem Anand Devarajan, A versatile route to synthesize MgO nanocrystals by combustion technique, Der. Pharma. Chemica. 3 (2011) 248-254.

[19] R. Subbiah, M. Veerapandian, K.S. Yun. Nanoparticles: Functionalization and Multi-functional Applications in Biomedical Sciences, Cur. Med. Chem. 17 (2010), 4559-4577.

[20] K. Kaviyarasu, Prem Anand Devarajan, A convenient route to synthesize hexagonal pillar shaped ZnO nanoneedles via CTAB surfactant, Adv. Mat. Lett. 4 (2013) 582-585.

Figure and Caption

Figure 1. XRD spectrum of MgO:AgO nanocube

Figure 2. Optical absorption images of MgO:AgO nanocube

Figure 3. Photoluminescence spectrum when excited at 350 nm

Figure 4. TGA/DTA pattern of MgO:AgO nanocube

Figure 5. μ-Raman spectrum of MgO:AgO nanocube

Figure 6. HRTEM and SAED analysis

Figure 7. XPS spectrum of MgO:AgO nanocube

Figure 8. Confocal laser scanning microscopic studies

Figure 9. Electrochemical behavior of MgO/AgO nanocube

Figure 10. Dielectric Studies of MgO:AgO nanocube

Figure 11. Atomic force microscopic studies of MgO:AgO nanocube

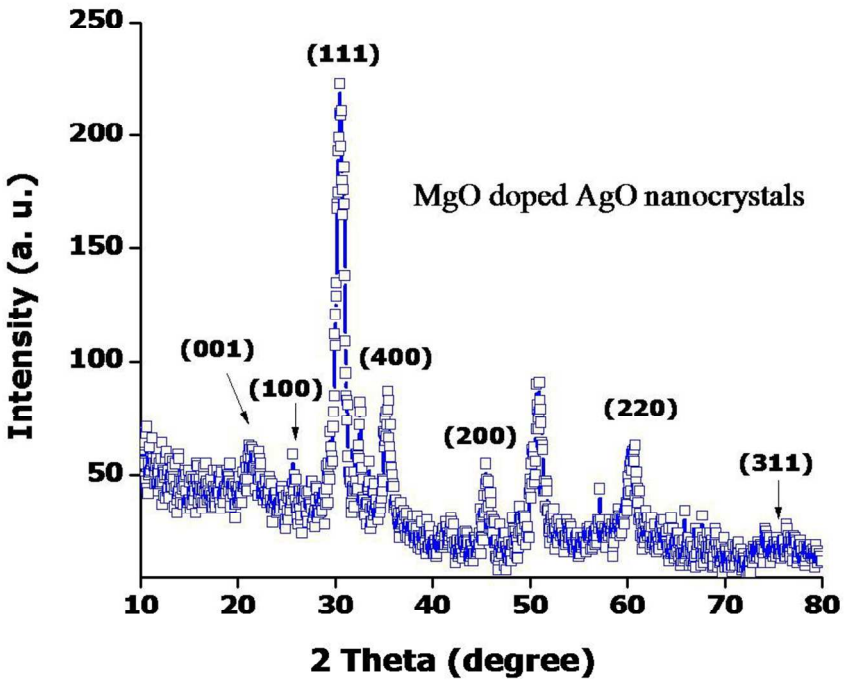

190x147mm (150 x 150 DPI)

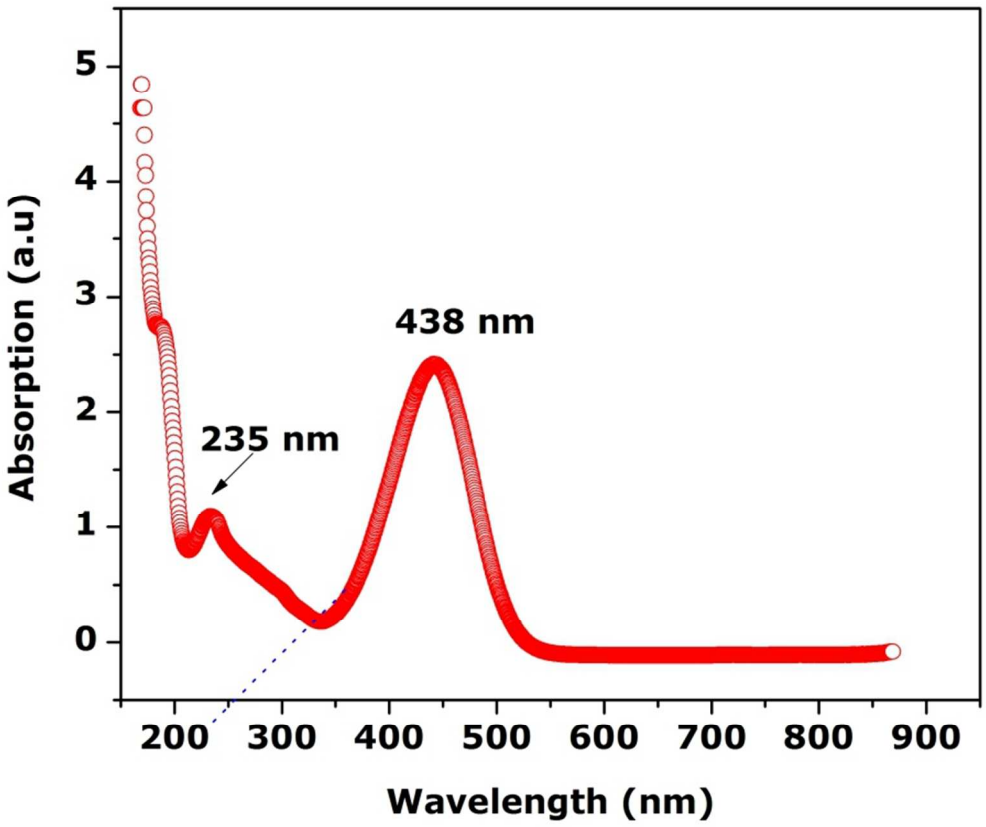

240x203mm (96 x 96 DPI)

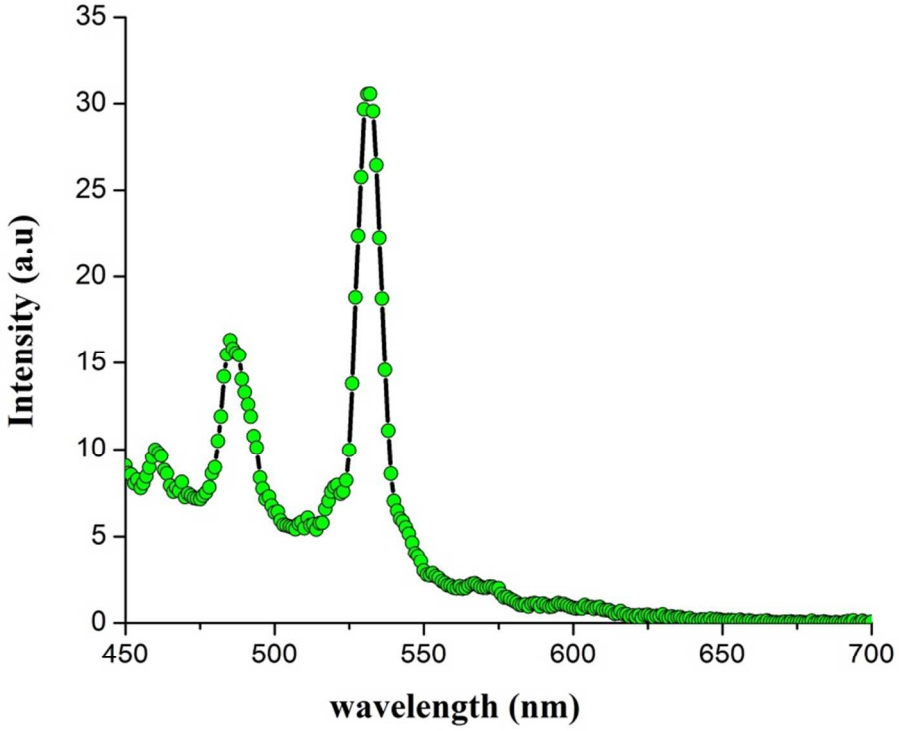

252x203mm (96 x 96 DPI)

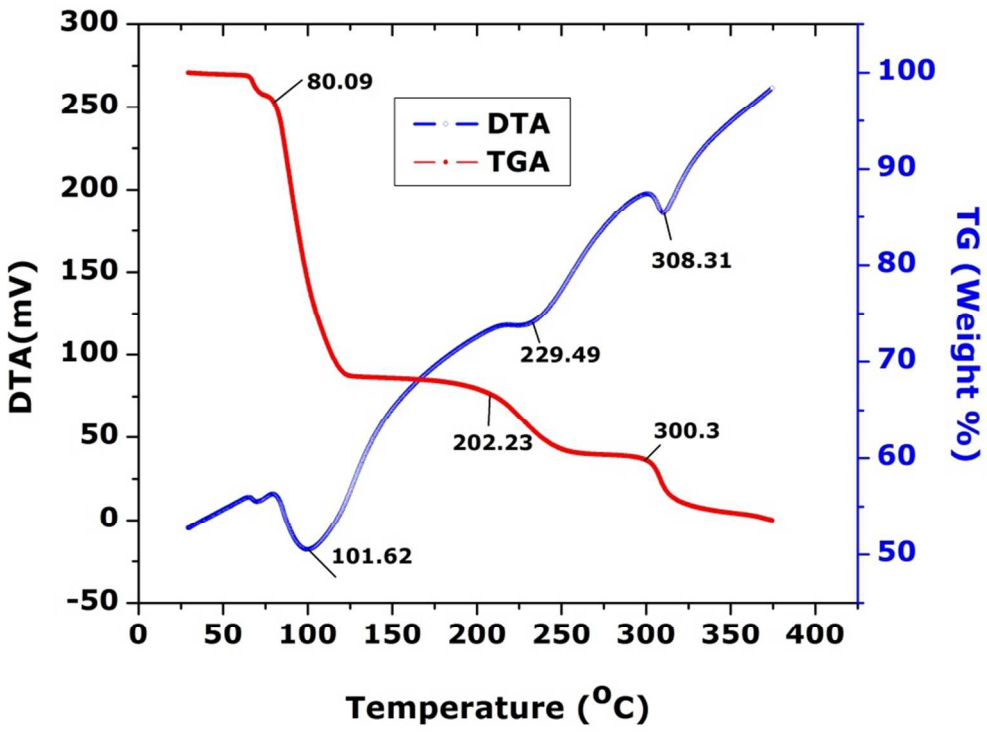

270x196mm (96 x 96 DPI)

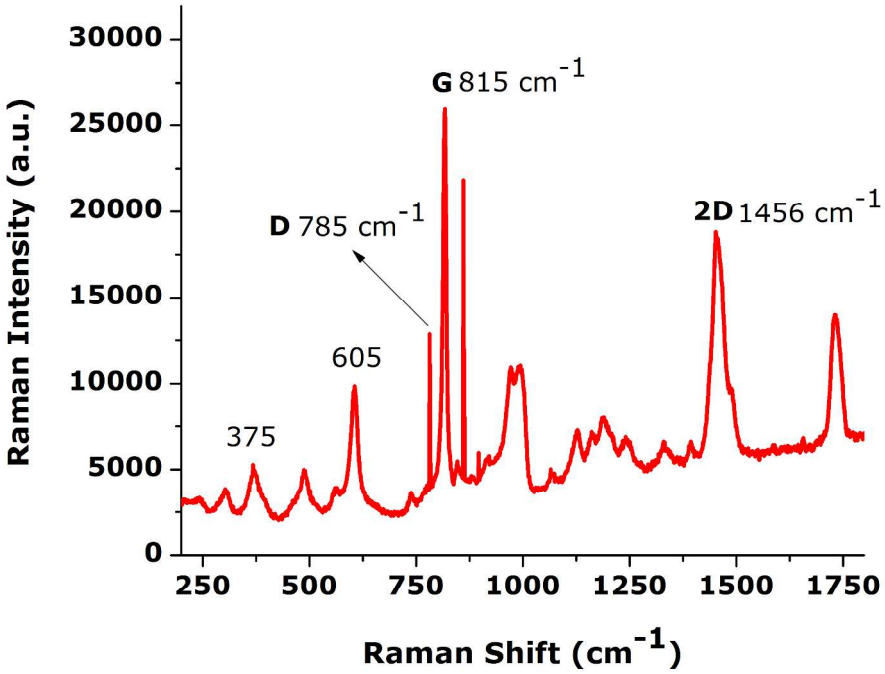

271x208mm (300 x 300 DPI)

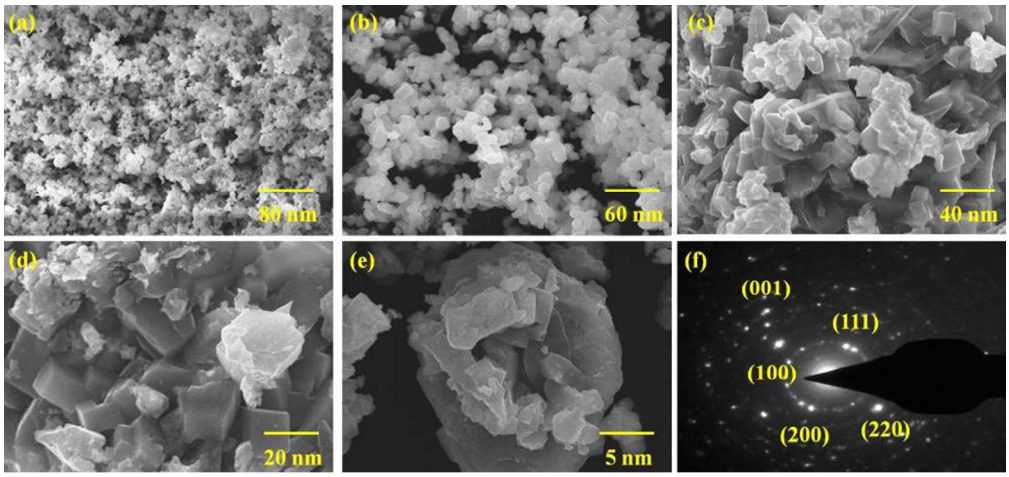

270x126mm (96 x 96 DPI)

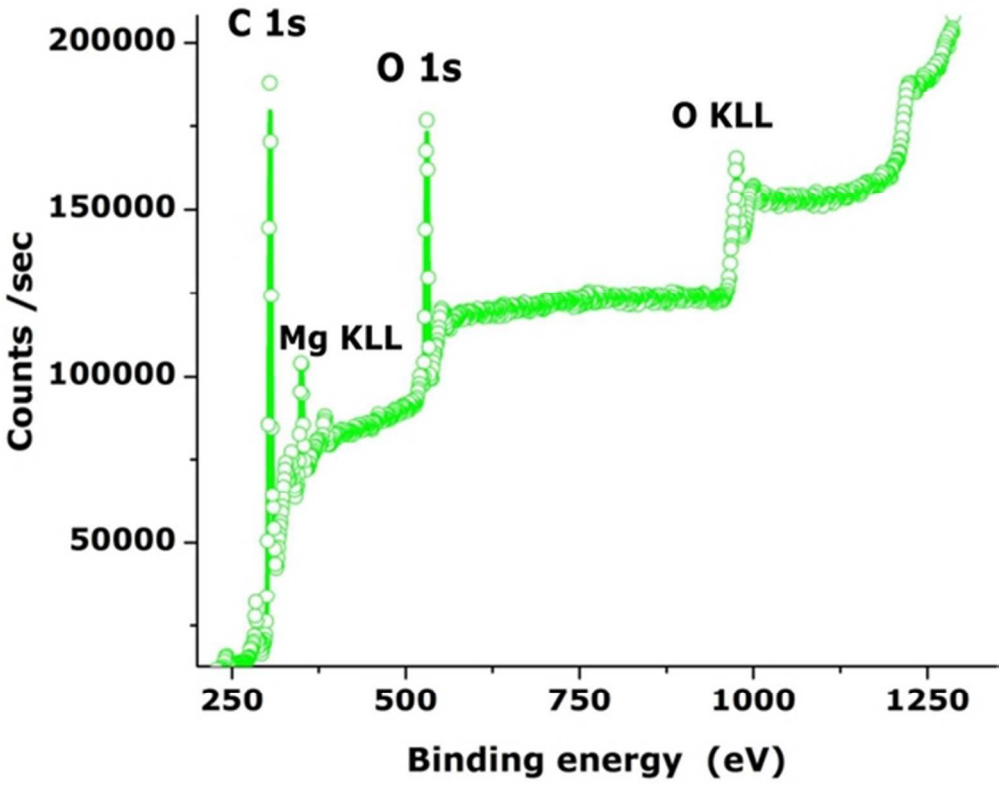

50x40mm (300 x 300 DPI)

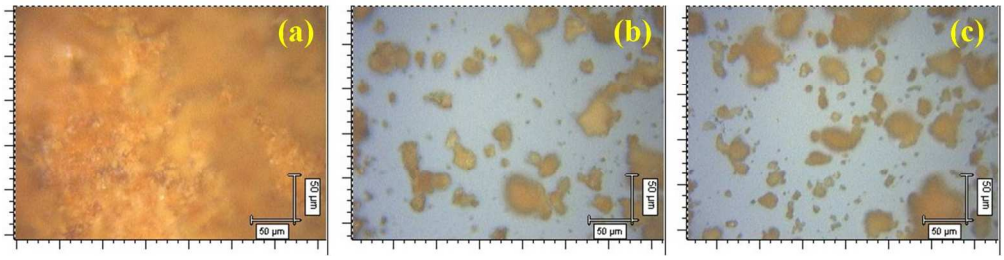

271x69mm (150 x 150 DPI)

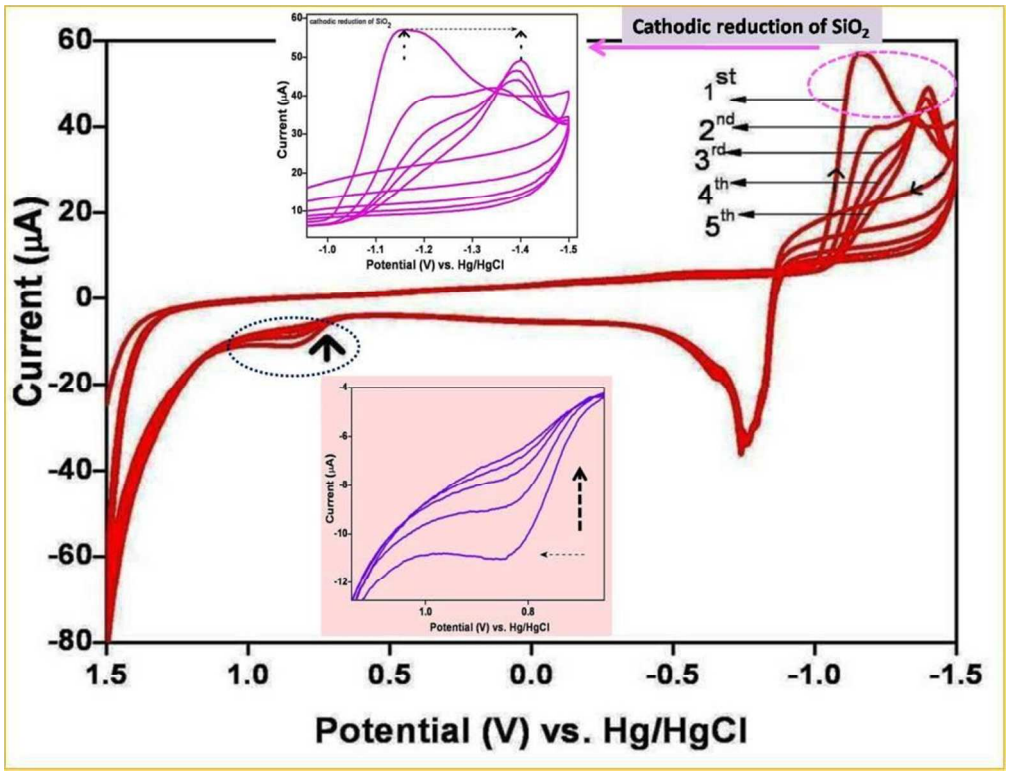

170x130mm (150 x 150 DPI)

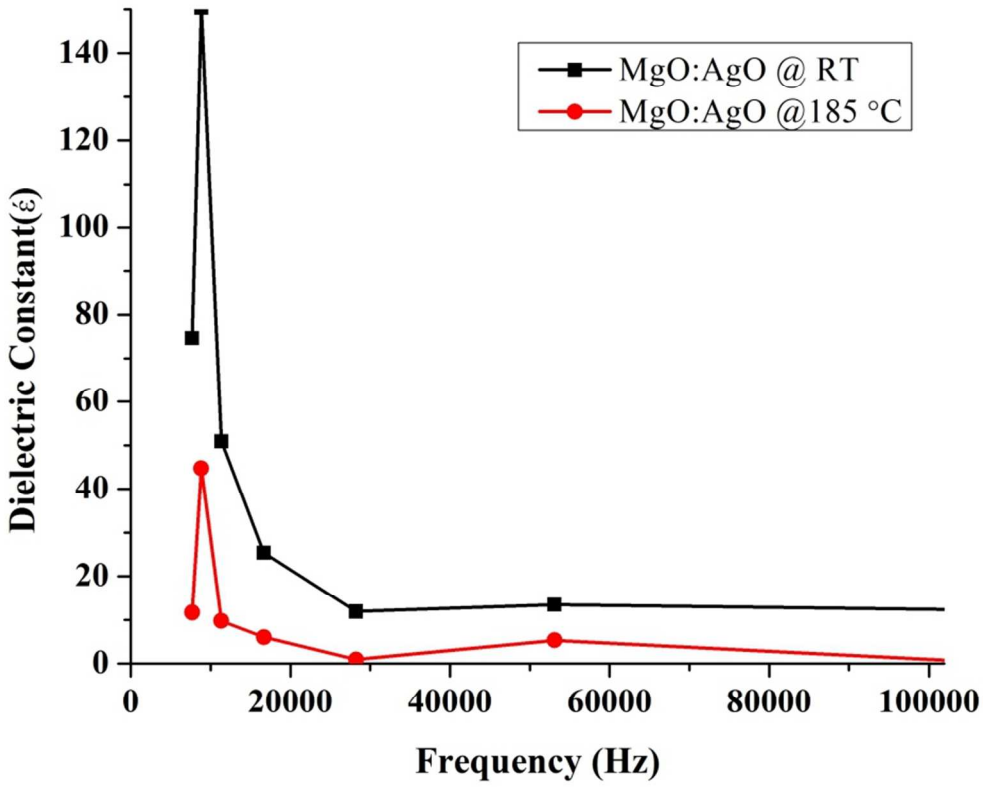

250x203mm (96 x 96 DPI)

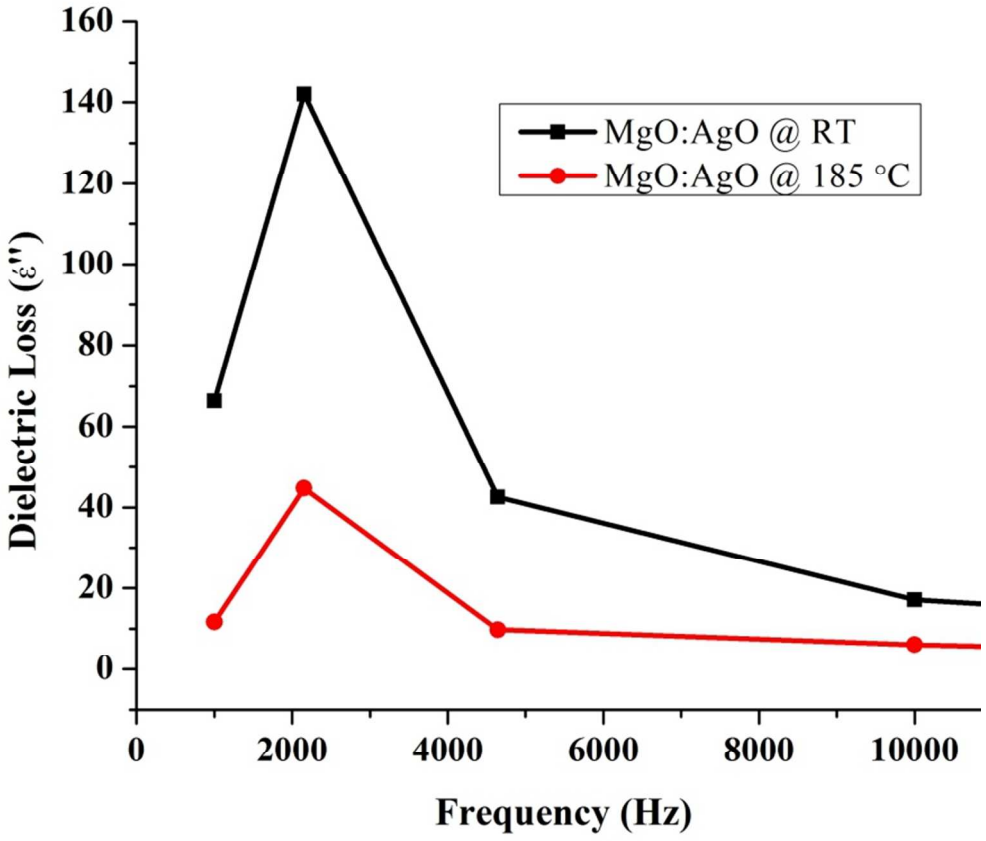

235x203mm (96 x 96 DPI)

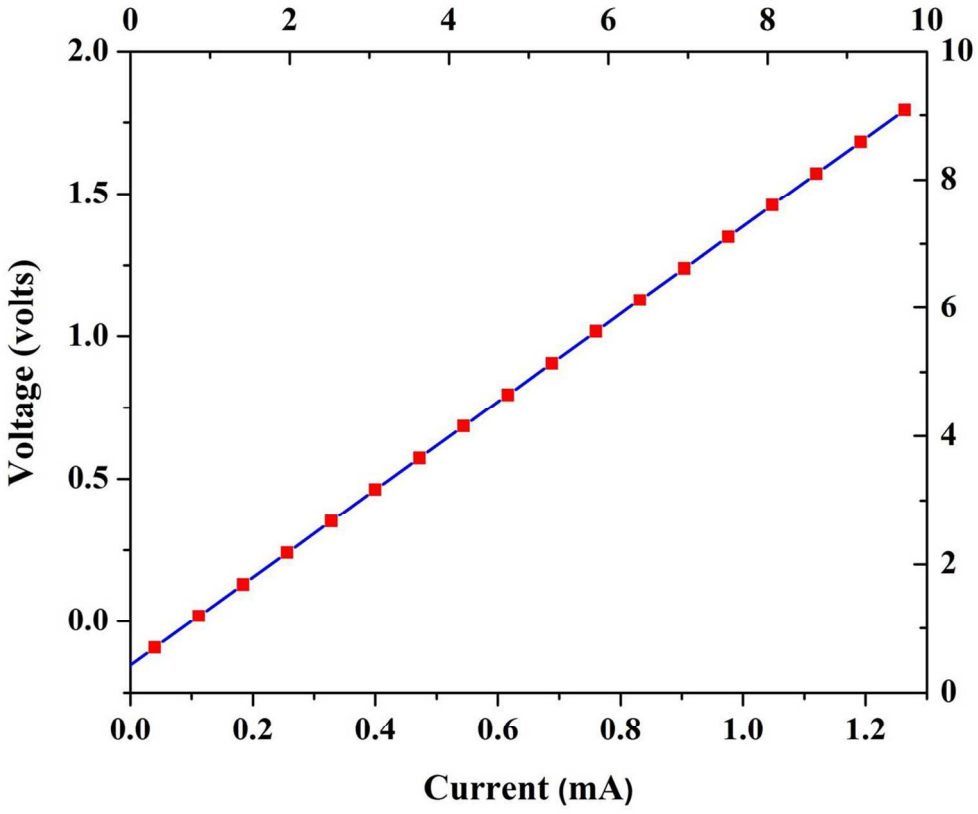

233x197mm (150 x 150 DPI)

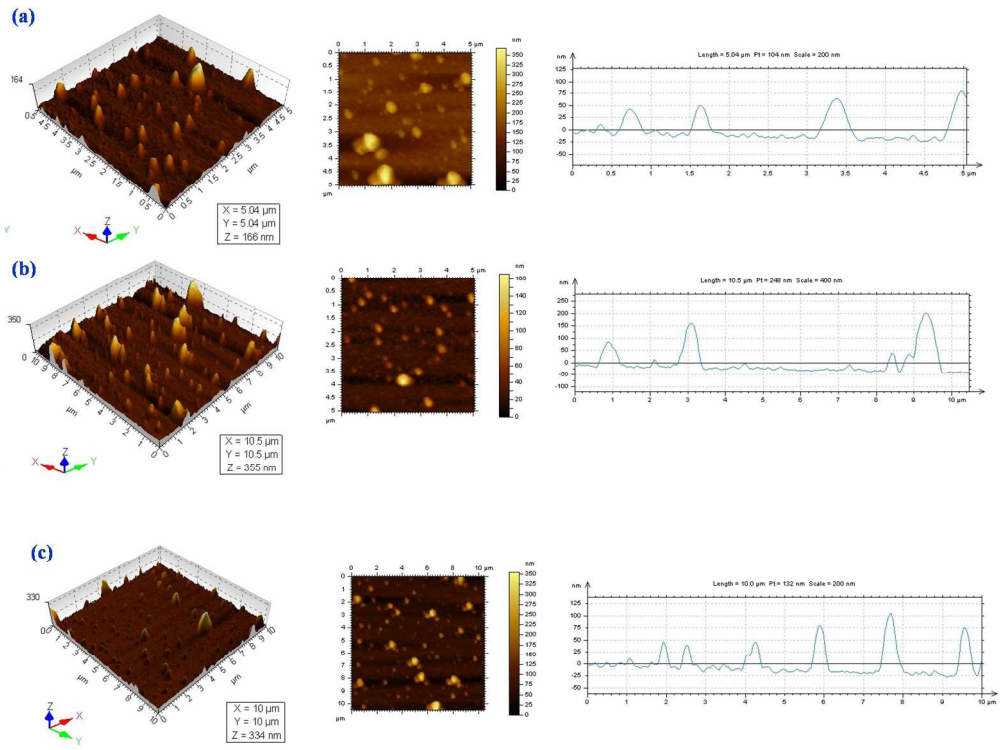

426x321mm (150 x 150 DPI)